ISSN 1063-7761, Journal of Experimental and Theoretical Physics, 2017, Vol. 125, No. 3, pp. 372–383. © Pleiades Publishing, Inc., 2017.
Original Russian Text © A.E. Afanasiev, P.N. Melentiev, A.A. Kuzin, A.Yu. Kalatskiy, V.I. Balykin, 2017, published in Zhurnal Eksperimental'noi i Teoreticheskoi Fiziki, 2017, Vol. 152, No. 3, pp. 438–452.

ATOMS, MOLECULES, OPTICS

# Quantum Transport of a Single Photon through a Subwavelength Hole by a Single Atom

**A. E. Afanasiev[a,*], P. N. Melentiev[a], A. A. Kuzin[a,b], A. Yu. Kalatskiy[a,b], and V. I. Balykin[a]**

[a] *Institute of Spectroscopy, Russian Academy of Sciences, Troitsk, Moscow, 108840 Russia*

[b] *Moscow Institute of Physics and Technology, Dolgoprudnyi, Moscow oblast, 141700 Russia*

**e-mail: afanasiev.isan@gmail.com*

Received March 20, 2017

**Abstract**—The localization and transport of a photon through a subwavelength hole with the help of a neutral atom are studied. A method proposed and realized in the study is based on the absorption of a photon by a neutral atom directly in front of a subwavelength hole, the flight of the atom through the hole, and photon emission on the other side of the screen. The influence of the interaction of the excited atom flying through the subwavelength channel with the screen material is estimated. The estimate showed that the atomic excitation can be quenched in holes with diameters smaller than 200 nm, which affects the photon transport efficiency.

**DOI:** 10.1134/S1063776117080131

## 1. INTRODUCTION

The efficient spatial localization of electromagnetic radiation is an important fundamental and applied problem. From the fundamental point of view, the spatial localization of light is of interest for studying the wave nature of radiation. In technological applications, the localization of light is necessary for overcoming the diffraction limit to increase the spatial resolution of optical instruments. The problems of the spatial localization of radiation are closely related to the problem of optical data communication. A communication channel should have not only high data transmission speed but also minimal size.

Various methods of radiation localization and information transfer can be quantitatively compared by introducing the localization efficiency coefficient $K_{\text{eff}}$ defined as the ratio of the length $l$ of the energy localization region, equal to the information transfer distance, to the transverse localization size $d$ determining the minimal size of required elements:

$$K_{\text{eff}} = \frac{l}{d}. \quad (1)$$

The greater this coefficient, the greater the information transfer distance for the minimal transverse size of the information channel. Figure 1 illustrates various approaches used for spatial localization of radiation and information (energy) transfer. The most obvious and simplest method for spatial localization of radiation is the use of a hole in an opaque screen. The modern version of this approach involves the use of a laser beam with the transverse spatial distribution formed in an optical cavity. In this case, the spatial energy localization in the micrometer range is achieved. However, the degree of spatial energy localization is restricted by diffraction losses. Optical radiation can be tightly focused into a spot of size $w_0 = f\lambda/\pi w$, where $f$ is the focal distance of a lens, $\lambda$ is the radiation wavelength, and $w$ is the size of a radiation spot on the lens. In this case, the characteristic size of the focal region is small and is determined by the Rayleigh length $z_R = \pi w_0^2/\lambda$, and the efficiency coefficient is determined by the expression $K_{\text{eff}} = \pi w_0/\lambda$. In the limiting tight-focusing case ($w_0 \approx \lambda/2$), we obtain the efficiency coefficient $K_{\text{eff}} \approx 1.6$.

The most popular method for spatial localization of radiation and its long-distance transfer uses the localization of radiation in optical fibers. The localization diameter in a single-mode fiber is determined by the diameter of its core $d \approx 8$ μm. The IR absorption of optical fibers is weak and the radiation propagation length in them achieves many kilometers. In this case, the efficiency coefficient (1) is determined by the ratio of the characteristic length on which energy decays $e$ times to the fiber core diameter and is $K_{\text{eff}} \approx 7 \times 10^9$.

In the case of a subwavelength hole, the spatial localization considerably increases; however, as was first shown by Bethe [1], the efficiency of radiation transfer through a subwavelength hole rapidly decreases for wavelengths exceeding the hole radius $r$ as $(r/\lambda)^4$, where $\lambda$ is the wavelength. In practice, a subwavelength hole is prepared in a finite-thickness screen, which additionally reduces the transmission

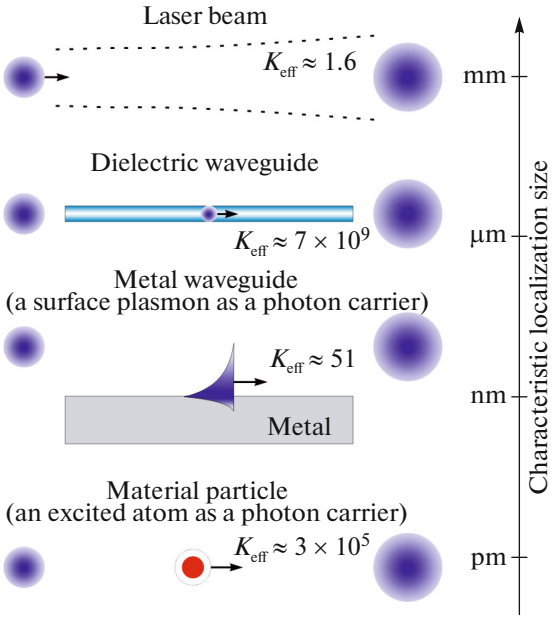


**Fig. 1.** (Color online) Methods of the spatial localization of radiation.

efficiency [2–5]. The transmission efficiency of such a hole can be increased with the use of photonic crystals [6] by locating the hole in the field of an optical Tamm state produced in a microcavity [7]. This approach provides an order of magnitude increase in the efficiency [8].

The discovery of the extraordinary transmission of light through a subwavelength hole in a finite-thickness metal screen [9] rekindled interest in studies of light transmission through subwavelength holes. The results of these studies contradict the standard diffraction theory. The following studies [10–13] have shown that a central role in the extraordinary light transmission effect belongs to surface waves such as surface plasmons representing electromagnetic waves on a metal surface localized due to their interaction with free electrons in metal [14]. In this case, radiation is localized on a nanometer spatial scale. For radiation in the optical range and a silver metal surface, the localization of a light wave is on the order of a hundred nanometers [15]. Metal nanowaveguides provide spatial localization of a few dozen nanometers. However, the propagation length of a plasmon wave does not exceed a few microns. In this case, the efficiency coefficient is $K_{\text{eff}} \approx 51$.

In this paper, we propose a new approach to the spatial localization of radiation energy and its efficient transport using material particles—namely, neutral atoms. This approach can reduce the spatial localization of the light wave energy to the atomic scale. In this case, as will be shown below, an atom moving in space can transfer the localized energy over large distances. In our experimental scheme, this distance is an order of 150 μm and is limited by the excited-state lifetime of the atom. In this case, the efficiency coefficient (1) is $K_{\text{eff}} \approx 3 \times 10^5$, which is much greater than in the case of laser radiation in free space and in the case of plasmonic waves. Note that the efficiency coefficient can be further increased up to its value achieved in optical fibers by using atoms in metastable states.

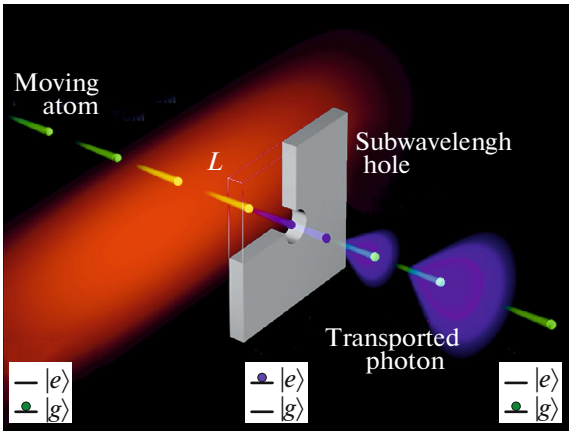


**Fig. 2.** (Color online) Basic idea of the localization of a single photon with the help of an atom and its transport through a subwavelength hole.

## 2. BASIC IDEA OF PHOTON LOCALIZATION AND TRANSPORT BY ATOMS

The basic idea of localization and transport of a single photon with the help of an atom is illustrated in Fig. 2. The moving atom absorbs a laser photon. In this case, the reduction of the wave packet of a single photon takes place resulting in localization of the electromagnetic energy on the atomic scale, which is considerably smaller than the radiation wavelength. The distance $l$ over which the atom can transfer the photon energy is determined by the excited-state lifetime. This distance depends on the atom velocity $v$ and its excited-state lifetime $\tau$, $l = v\tau$, and can achieve several dozen millimeters when atoms in metastable states with lifetimes $\tau \approx 100$ μs and thermal velocities $v \approx 300$ m/s are used.

In the classical treatment, the spatial localization of the photon energy by an atom is determined by the physical size of the atom. In the rigorous quantum-mechanical consideration, it is necessary to take into account the wave properties of a material particle, which will determine the size of the spatial localization of the photon energy.

For material particles, as in the case of electromagnetic waves, the probability that an atomic particle will pass through a subwavelength hole decreases as the de Broglie wavelength approaches the hole size. The probability that an atom will pass through a hole with

diameter much smaller than the de Broglie wavelength of the atom is negligibly small. For example, for cold atoms with temperature about 1 μK and, correspondingly, having the de Broglie wavelength about 1 μm, the probability of an atom passing through a hole a fraction of micron in size is negligibly small, although the atom (considered classically) is substantially smaller than the hole size. For atoms with thermal velocities, the corresponding de Broglie wavelengths lie in the subnanometer range and, for the hole dimeter down to a few dozen nanometers, the wave nature of the atom does not play a substantial role.

We will show below that the proper choice of the hole size, atom velocity, and the excitation wavelength of the atom can provide efficient photon transport through a subwavelength hole. Note that the experimental realization of photon transport is restricted by a number of factors related to the interaction of the excited atom with the surface of the hole screen, which will be considered below.

The localization of the photon energy and its transport by an atom can be performed in experiments with atoms flying through a subwavelength hole, as shown in Fig. 2. If the atom lifetime considerably exceeds the characteristic time of flight through the hole (this is a channel in real experiments), the transition of the atom from the excited to ground state with the photon emission can, under certain conditions, occur on the other side of the screen, which means the localization and transport of the photon energy.

Let us compare the efficiency of photon transport by an atom through a subwavelength hole with the efficiency of transmission of "a free photon" in a laser beam incident on the hole. It was shown in [16] that the ratio of the probability $P_{\text{atom}}$ of transmission of a photon with the wavelength $\lambda$ through a subwavelength hole with radius $r$ with the participation of an atom to the photon transmission probability $P_{\text{hole}}$ without an atom is determined by the cross section $\sigma_{\text{hole}}$ for photon scattering by the hole and the atom excitation cross section $\sigma_{\text{atom}}$ and is

$$\zeta = \frac{P_{\text{atom}}}{P_{\text{hole}}} \sim \frac{\sigma_{\text{atom}}}{\sigma_{\text{hole}}} \sim \left(\frac{\lambda}{r}\right)^6. \quad (2)$$

For the radiation wavelength $\lambda = 800$ nm and the hole radius $r = 50$ nm, the ratio of photon transfer probabilities is $\zeta \approx 2 \times 10^4$. Thus, the efficiency of photon transport by an atom can be many orders of magnitude higher than the probability of transport of "a free photon" through a nanohole. Such a high photon transport probability is caused by the reduction of the wave packet of a single photon due to its absorption by the atom resulting in its localization in a volume with the characteristic size much smaller than the radiation wavelength and the subwavelength hole. The single-photon single-mode wave packet of laser light is transformed to a single-photon multimode wave packet in a free space. Because the atom emission occurs spontaneously after its flying through the subwavelength hole, the absorbed and emitted photons cannot be considered identical. In the process under study, the atom transfers only the energy of a single photon.

The probability ratio (2) is obtained in the ideal case of the interaction of a single atom located near a subwavelength hole with a single photon in resonance with a certain laser radiation mode. In real experiments, the probability of excitation of a single atom by a single photon is extremely small even when radiation is focused into a spot of size smaller than the absorption cross section $\sigma_{\text{atom}}$ of the atom [17]. Note that the atom excitation effectivity can be increased by using a light pulse identical to the light pulse of a spontaneous photon emitted by the atom [18], which is very difficult upon excitation of atoms in a thermal beam.

Aside from fundamental physical limitations on the experimental realization of photonic transport by an atom, a number of technical limitations also appear, such as the background laser radiation during the registration of the atom flight, radiation from excited atoms in front of the screen, and some other limitations considered below.

## 3. CHOICE OF AN ATOM AND ITS EXCITATION SCHEME

One of the main parameters determining the length of photon transfer by an atom is the excited-state lifetime of the atom. We used Rb atoms in our experiments. Consider the energy level diagram of the Rb atom (Fig. 3a) from the point of view of the optimal choice of the energy state for realizing photon transport by the atom. If a thermal atomic beam excited with 780 nm on the transition $5S_{1/2} \rightarrow 5P_{3/2}$ with a lifetime of the excited state of about 27 ns is used, the expected transfer length is about 8 μm. The photon transfer over such a short distance is difficult to perform and therefore atomic levels with longer lifetimes should be used.

To increase the photon transport length, it is convenient to use the $5D_{5/2}$ state with the lifetime 240 ns. The atom can be excited to the $5D_{5/2}$ state by the two-step scheme [19]: at the first step, the atom is excited at the $5S_{1/2} \rightarrow 5P_{3/2}$ transition by a laser at 780 nm and at the second step – at the $5P_{3/2} \rightarrow 5D_{5/2}$ transition by a laser at 776 nm. One can see from the energy level diagram of the Rb atom that the $5D_{5/2}$ state has several decay channels. In the $5D_{5/2} \rightarrow 6P_{3/2} \rightarrow 5S_{1/2}$ decay channel, blue photons are emitted at 420 nm and it is appropriate to detect the photon transport at this wavelength. In this case, a great difference between excitation (780 and 776 nm) and fluorescence (420 nm) wavelengths allows one to suppress (with the help of optical filters) the background radiation of exciting laser fields, which is partially transmitted through a subwavelength hole.

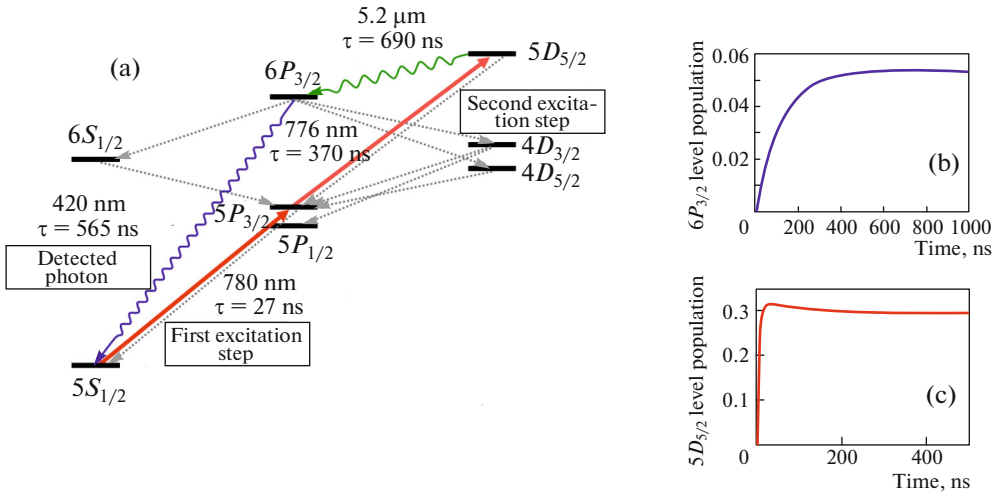


**Fig. 3.** (Color online) (a) Energy level diagram of a Rb atom. The red arrows show atomic transitions for exciting the atom to the long-lived $5D_{5/2}$ state. The green arrow shows the decay of the $5D_{5/2}$ state to the $6P_{3/2}$ state from which the atom undergoes a transition to the ground state emitting a blue photon at 420 nm. (b, c) The time dependences of the population of the $5D_{5/2}$ and $6P_{3/2}$ states during laser excitation.

We analyzed the excitation of atoms to the $6P_{3/2}$ state and subsequent spontaneous transitions from the excited to ground state by calculating the temporal population dynamics of atomic states excited by the two-frequency laser field. Calculations were performed both quantum-mechanically using the density matrix and by the quasi-classical method using the rate equations. Both these approaches gave comparable results on the population dynamics of the $5S_{1/2}$, $5P_{3/2}$, $5D_{5/2}$, and $6P_{3/2}$ states. Calculations showed that for large saturation parameters for both transitions $5S_{1/2} \to 5P_{3/2}$ and $5P_{3/2} \to 5D_{3/2}$, atoms can be efficiently excited to the $5D_{5/2}$ state [20].

Consider the population dynamics of the energy levels of rubidium atoms calculated by solving the rate equations. The rate equations have the form

$$\begin{aligned}
\dot{n}_{5S}(t) &= A_{6P5S}n_{6P}(t) + (A_{5P} + B_{5P5S}W_{780}) \\
&\times n_{5P}(t) - B_{5S5P}W_{780}n_{5S}(t), \\
\dot{n}_{5P}(t) &= B_{5S5P}W_{780}n_{5S}(t) - B_{5P5D}W_{776}n_{5P}(t) \\
&+(A_{5D5P} + B_{5D5P}W_{776})n_{5D}(t) - (A_{5P} + B_{5P5S}W_{780})n_{5P}(t), \\
\dot{n}_{5D}(t) &= B_{5P5D}W_{776}n_{5P}(t) \\
&-(A_{5D} + B_{5D5P}W_{776})n_{5D}(t), \\
\dot{n}_{6D}(t) &= A_{5D6P}n_{5D}(t) - A_{6P}n_{6P}(t), \\
\dot{n}_{4D}(t) &= A_{6P4D}n_{6P}(t) - A_{4D}n_{4D}(t), \\
\dot{n}_{6S}(t) &= A_{6P6S}n_{6P}(t) - A_{6S}n_{6S}(t),
\end{aligned} \tag{3}$$

where $n_{5S}$, $n_{5P}$, $n_{5D}$, $n_{6P}$, $n_{4D}$, and $n_{6S}$ are populations of corresponding levels, $A$ and $B$ are the Einstein coefficients related to the rates of spontaneous and stimulated transitions between corresponding levels; $W_{780}$ and $W_{776}$ are the electromagnetic field densities at wavelengths 780 and 776 nm, respectively. Figures 3b and 3c show the time dependence of the populations of atomic states $6P_{3/2}$ and $5D_{5/2}$ excited by a laser field, which were obtained from the numerical solution of rate equations laser excitation intensities used in experiments (presented below). The calculation showed that the atom undergoes a transition from the $5D_{5/2}$ state to the $6P_{3/2}$ state with probability 35% and then to the ground $5S_{1/2}$ state with probability 31% by emitting a photon at 420 nm [21, 22]. Calculations showed that the excitation time of the atom in the $5D_{5/2}$ state is $\tau_1 \approx 50$ ns. This time restricts the minimal size of the excitation region in front of the screen, which should be greater than $l = v\tau_1 \approx 15$ μm.

The solution of rate equations with initial conditions $n_{5S}(t=0) = 0$, $n_{5P}(t=0) = 0$, $n_{5D}(t=0) = 1$, $n_{6P}(t=0) = 0$, $n_{4D}(t=0) = 0$, and $n_{6S}(t=0) = 0$ gives the photon emission time at the 420-nm $6P_{3/2} \to 5S_{1/2}$ transition. The results of this calculation are presented in Fig. 4. The $5D_{5/2} \to 6P_{3/2} \to 5S_{1/2}$ decay of the $5D_{5/2}$ state with emission of a photon at 420 nm occurs with the decay time 500 ns. Such a long lifetime provides the transfer of the photon energy by the atom over a distance of about 150 μm. This value is sufficient for the flight of the excited atom through a subwavelength hole in a screen and for efficient laser excitation of the atom to the $5D_{5/2}$ states in front of the screen. Note that a consideration of the efficiency of excitation to the $5D_{5/2}$ state shows that only 2% of all atoms flying through the excitation region emit blue photons at 420 nm. This value restricts the photon transfer efficiency by the atom in this scheme.

An important parameter of the efficiency of photon transport by the atom is the ratio of the number of photons transferred by atoms to the number of photons transmitted through the subwavelength hole

without the participation of atoms. To determine the efficiency, we will estimate the number of photons that can be transferred through a single subwavelength hole by a flux of excited atoms. The number of atoms incident on a single hole with area $S$ per unit time is $N^{\text{atom}} = FS$, where $F$ is the atomic flux. Each atom can transfer no more than one photon, and the number of photons transferred by atoms will be

$$N_{\text{atom}}^{\text{photons}} = \eta N^{\text{atoms}} = \eta FS, \tag{4}$$

where $\eta$ is the photon transfer efficiency. The parameter $\eta$ is determined by the excitation efficiency of an atom in front of the screen and the probabilities of relaxation of excited atoms over all possible decay channels. In the case of a two-level atom, the maximum value of the parameter $\eta = 1$ appears when the population inversion is achieved. In the case of Rb atoms in the excited $5D_{5/2}$ state, this coefficient is 2%.

The photon transfer by atoms can be efficiently performed using a flux of thermal atoms incident on a screen with subwavelength holes. The maximal atomic flux in an effusion beam is $F \approx 10^{14}$ at/(s cm$^2$). For such an atomic flux and the hole radius 50 nm, the maximum possible number of transferred photons is extremely small $N_{\text{atom}}^{\text{photons}} = 7.9 \times 10^3$ photon/s.

To excite atoms efficiently, the laser radiation intensity should be equal to the saturation intensity of the atomic transition. Consider the interaction of an atom with electromagnetic radiation. The probability of population of an excited level in the stationary state is

$$\rho_{ee} = \frac{I/I_{\text{sat}}}{1 + 4(\Delta/\Gamma)^2 + I/I_{\text{sat}}}. \tag{5}$$

In the case of resonance excitation of atoms ($\Delta = 0$) and the absence of the excited state relaxation caused by atom–surface interaction, the coefficient $\eta = \rho_{ee} = 0.25$.

Laser photons exciting atoms also propagate through the hole. Consider the excitation of atoms by a laser field normally incident on a screen with a subwavelength hole. In this case, according to the Bethe theory, the number of photons transmitted through the hole is determined by the expression

$$N_{\text{atom}}^{\text{photons}} = \frac{I\sigma_{\text{hole}}}{\hbar\omega}, \tag{6}$$

where, according to the Bethe theory,

$$\sigma_{\text{hole}} = \frac{1024\pi^3 r^6}{27\lambda^4}. \tag{7}$$

Let us determine the ratio of the number of photons transported by atoms to the number of photons transmitted through the subwavelength hole without the participation of atoms. The intensity of excitation field is $I = I_{\text{sat}}$. The saturation intensity is described by the expression $I_{\text{sat}} = \hbar\omega\Gamma/2\sigma_{\text{atom}}$, where the resonance absorption cross section for the atom is $\sigma_{\text{atom}} = 3\lambda^2/2\pi$. Using expressions (4)–(6), we obtain

$$k = \frac{N_{\text{atom}}^{\text{photons}}}{N_{\text{hole}}^{\text{photons}}} = \frac{\eta FS}{I_{\text{sat}}\sigma_{\text{hole}}/\hbar\omega} = \frac{1}{2}\frac{F\pi r^2\sigma_{\text{atom}}}{\Gamma\sigma_{\text{hole}}} = \frac{81}{4096}\frac{F}{\Gamma\pi^3}\frac{\lambda^6}{r^4}. \tag{8}$$

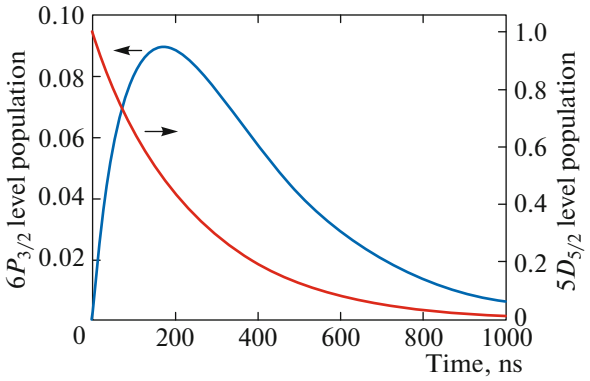


**Fig. 4.** (Color online) Time dependences of populations of the $5D_{5/2}$ (red curve) and $6P_{3/2}$ (blue curve) levels of the Rb atom during the decay from the $5D_{5/2}$ state. The $5D_{5/2} \rightarrow 6P_{3/2} \rightarrow 5S_{1/2}$ decay with emission of photons at 420 nm has the decay time about 500 ns.

Figure 5a shows the dependences of the number of photons transferred by atoms calculated by (4) and the number of photons (6) transmitted through the hole without an atom on the hole radius. The atomic flux was taken to be $F = 10^{14}$ at./(s cm$^2$). Figure 5b shows the dependence of the coefficient $k$ on $r$ obtained from (8). Calculations were performed for excitation parameters $\lambda = 780$ nm, $I_{\text{sat}} = 1.6$ mW/cm$^2$, and $\Gamma = 2\pi \times 6$ MHz, corresponding to the $D2$ line of rubidium atoms. The calculations show that the efficiency of photon transfer by an atom strongly depends on the hole size. A significant advantage in the efficiency can be obtained only for holes with $r < 40$ nm.

The low efficiency of photon transfer by atoms under real experimental conditions is explained by a great difference in the atomic and photon fluxes incident on the screen. The increase in the atomic flux leads to the increase in the transfer efficiency. However, the increase in the atomic flux is a complicated technological problem.

The estimates presented above show that the use of exciting laser radiation normally incident on the screen surface in experiments on the transfer of photons by atoms through subwavelength holes leads to a considerable parasitic signal. Therefore, the use of exciting laser radiation propagating parallel to the screen plane is preferable. In this case, $\sigma_{\text{hole}} \rightarrow 0$ and, according to (8), the coefficient $k \rightarrow \infty$, which provides the efficient atom-assisted photon transport through a hole of any diameter.

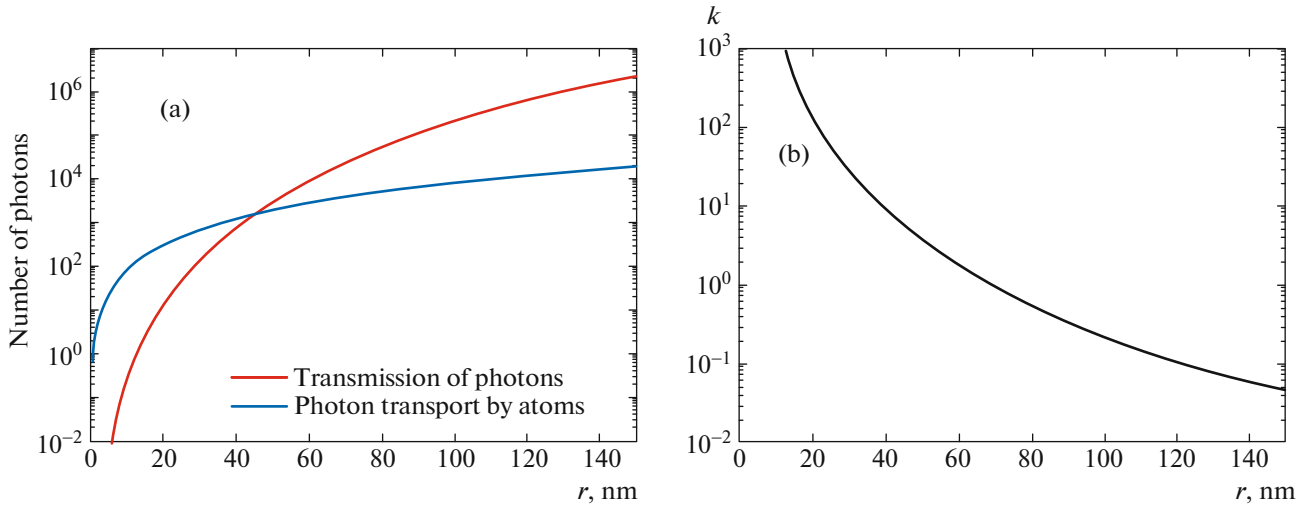


**Fig. 5.** (Color online) Efficiency of photon transport by atoms through a subwavelength hole: (a) the number of photons transported by atoms (blue curve) and the number of photons transmitted through a subwavelength hole without participation of atoms (red curve); (b) the ratio of the number of photons transported by atoms to the number of photons transmitted without participation of atoms calculated by (8).

## 4. EXPERIMENTAL DEMONSTRATION OF PHOTON ENERGY TRANSFER BY AN ATOM

The photon transport by an atom in the excited state through a subwavelength hole was demonstrated in a scheme shown in Fig. 2. A Rb atomic beam in a vacuum chamber intersected at a right angle an exciting laser beam. The flux of rubidium atoms from an atomic oven was formed by a set of apertures. For the temperature of the atomic source 140°C, the atomic beam intensity was $F = 2 \times 10^{13}$ at. s/cm$^2$. Atoms were excited directly in front of the screen using the two-stage scheme (Fig. 3) involving excitation of Rb atoms from the ground $5S_{1/2}$ state via the intermediate $5P_{3/2}$ state to the $5D_{5/2}$ state ($5S_{1/2} \rightarrow 5P_{3/2} \rightarrow 5D_{5/2}$). This was performed using two diode lasers. The first one emitting at 780 nm excited atoms at the $5S_{1/2} \rightarrow 5P_{3/2}$ transition. This laser was frequency-stabilized using saturated absorption spectroscopy with an external cell containing rubidium atoms vapors. The second laser emitting at 776 nm excited atoms at the $5P_{3/2} \rightarrow 5D_{5/2}$ transition. The emission frequency of the second laser was stabilized with the help of a high-finesse Fabry–Perot etalon. The measurement and control of the wavelengths of lasers and their radiation frequency tuning were performed using a hugh-precision λ-meter. The size of the laser excitation region was 90 μm. After excitation of an atom to the $5D_{5/2}$ state, the atom experienced a transition to the $5S_{1/2}$ ground state emitting spontaneously a photon at 420 nm, which was detected with an avalanche photodiode or a two-dimensional CCD camera.

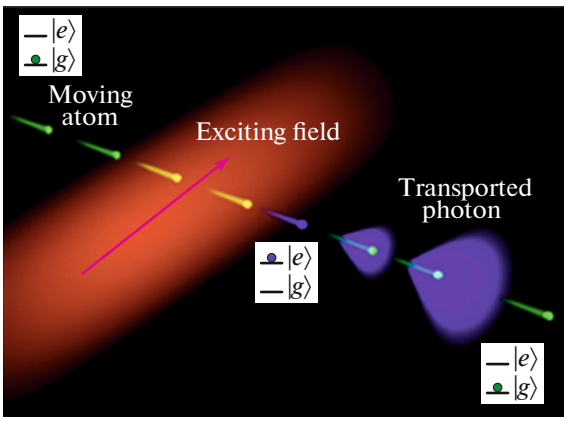


**Fig. 6.** (Color online) Scheme of the experiment on studying the spatial photon energy transfer by an excited atom in a free space.

First we measured the excitation dynamics of atoms followed by their deexcitation with emission of photons (without a screen with a hole) (Fig. 6). Atoms were excited by pulsed laser radiation ($\tau$ = 300 ns; $\Delta = 780$ nm) produced with the help of an acoustooptic modulator (AOM). Fluorescence from atoms at 420 nm was detected for different delay times with respect to the exciting pulse (Fig. 7a).

Figure 7b shows the dependence of the fluorescence signal of atoms on the time delay of their excitation. Measurements were performed for atoms freely moving in a vacuum chamber and for atoms colliding with a surface after interaction with the laser field. The deexcitation probability of atoms in collisions with a surface was measured with a glass substrate with a deposited 20-nm thick chromium layer oriented perpendicular to the atomic beam. The distance from the

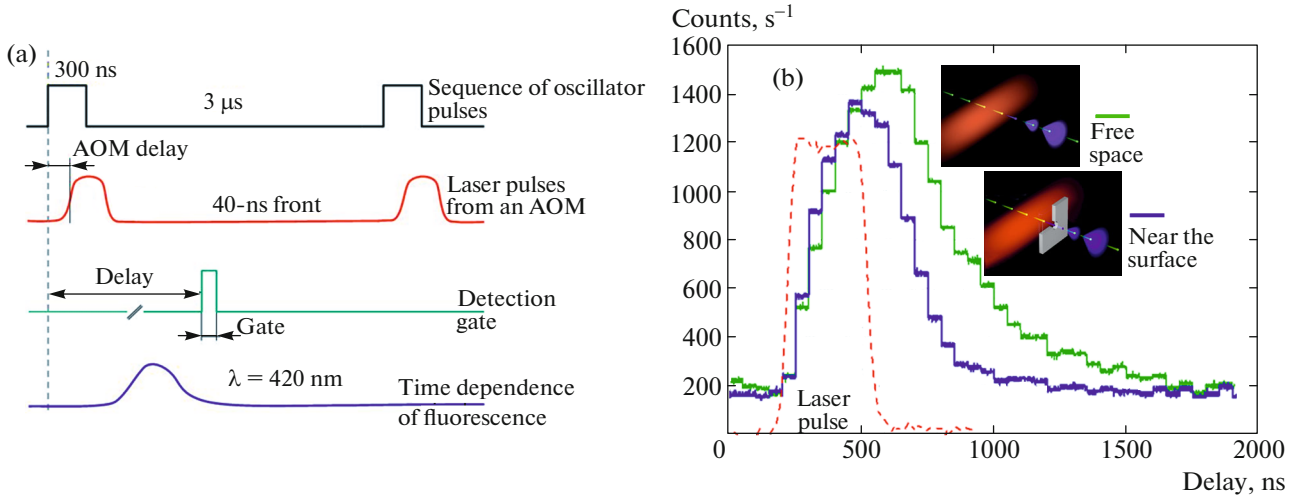


**Fig. 7.** (Color online) Time distribution of a fluorescence signal upon pulsed excitation of flying atoms: (a) the time pump–probe sequence; (b) time distributions of a fluorescence signal upon excitation in a free space and near a surface.

exciting laser beam to the substrate surface was 100 μm.

The plots in Fig. 7b show that the maximum of the fluorescence signal is shifted with respect to the excitation pulse by approximately 200 ns. This is explained by the delay in population of the $6P_{3/2}$ state of the atom. The shape of the fluorescence signal repeats the calculated dependence in Fig. 4.

The fluorescence dynamics of atoms moving to the surface and excited in front of it is different because they are deexcited in collisions with the substrate surface. This can be seen in the dependence of the fluorescence signal (Fig. 7b) showing the signal decrease at large times.

To visualize the spatial energy transport by atoms, we studied the spatial dependence of fluorescence. The excitation and relaxation regions of atoms were imaged on a two-dimensional CCD with the help of a high-numerical aperture objective. Figure 8 presents the experimental and calculated spatial distributions of fluorescence of a moving atom at a wavelength of 420 nm. One can see (Fig. 8b) that the fluorescence region is displaced with respect to the excitation region, which is explained by the delay in the population of the $6P_{3/2}$ level (see Figs. 3 and 7b). Figure 8 also shows the exponentially decaying fluorescence signal. The decay occurs at the characteristic scale 150 μm coinciding with the photon transport length calculated earlier and determined by the decay of the excited state of the atom.

Figure 8a presents the results of numerical calculations using the rate equations of the spatial distribution of fluorescence during the flight of atoms through the excitation region (shown by the dashed curve) 90 μm is size. Calculations took into account the Maxwell velocity distribution of atoms. Theoretical curves completely coincide with experimental data.

## 5. EXPERIMENTAL DEMONSTRATION OF THE SPATIAL LOCALIZATION OF THE PHOTON ENERGY BY AN ATOM

To demonstrate the spatial localization of the photon energy by an atom, we studied the flight of the excited atom through nanoholes with different diameters. The scheme of the experiment is shown in Fig. 2. The atom moves to a screen with a nanohole and absorbs a laser photon directly in front of the screen. If the lifetime of the excited atom considerably exceeds its flight time through the hole (in real experiments, through a channel), the atom can undergo a transition from the excited to ground state with emission of a photon on the other side of the screen, which means the photon energy transfer through the nanohole. The detection of a photon emitted by the atom on the other side of the screen will indicate the localization of the absorbed photon energy to the transverse size smaller than the hole diameter.

The photon energy transfer by an excited atom through a nanohole was first demonstrated in [16], where it was shown that the spatial localization of radiation at the atomic scale does occur in this process.

As mentioned above, one of the main parameters determining both the efficiency of photon transfer by an atom thorough a subwavelength hole and the experimental possibility of this process at all is the lifetime of the excited atom. The lifetime of the excited state of atom $\tau$ should exceed the time of flight of an atom through a subwavelength hole channel in a finite-thickness screen ($\tau > h/v$, where $h$ is the screen thickness and $v$ is the velocity of atoms). The increase in the lifetime of the atom in the excited state reduces the

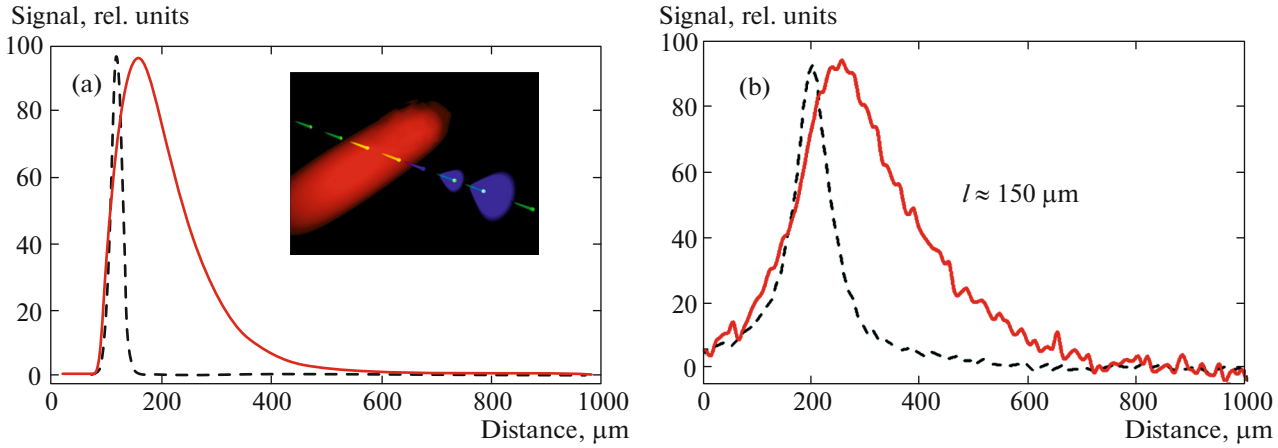


**Fig. 8.** (Color online) Spatial distribution of a fluorescence signal at 420 nm during the flight of atoms through the excitation region of width 90 μm: (a) theoretical curve; (b) experimental curve. The dashed curve shows the regions of excitation by laser radiation.

probability of the decay of this state in front of the screen, which in turn reduces the number of reemitted spontaneous photons in front of the screen and, accordingly, leads to an increase in the distance to which the atom is able to transport the photon. The photons emitted in front of the screen can propagate through nanoholes (without the participation of atoms) and determine the background signal in the measurement of the photon transport by the atom. The number of background photons depends both on the lifetime of the atom and the excitation region size $l$ in front of the screen and is $N_{bkg} \sim l/v\tau$. It follows from this expression that, for a finite excitation region of the atom (determined by the necessary condition for the high excitation efficiency), the decrease in the lifetime leads to the increase in the reemission of photons by the atom in front of the screen, which in turn determine the background signal.

We demonstrated the photon energy localization in experiments with photon transport by an atom through an array of subwavelength holes with different diameters made in an opaque screen. The hole array was made in a 40-nm thick $SiO_2$ membrane covered with a thin silver film. Subwavelength holes in the metal film–membrane screen were produced by a tightly focused $Ga^+$ ion beam. Through holes with diameters from 55 nm to 6 μm were made. The screen with nanoholes was prepared in two stages: (1) A 20-nm thick silver film required for producing holes by an ion beam was deposited on a $SiO_2$ membrane; (2) after the preparation of an array of subwavelength holes, a 190-nm thick silver film was additionally deposited to increase the optical density of the screen. The total screen thickness was 250 nm. We made arrays of through holes with the following parameters: (a) the hole diameter $d = 175$ nm and array period $T = 1.6$ μm; (b) $d = 260$ nm, $T = 2$ μm; (c) $d = 400$ nm, $T = 2$ μm; (d) $d = 480$ nm, $T = 2.5$ μm; (e) $d = 540$ nm, $T = 2.5$ μm.

Aside from subwavelength holes, control microholes 6 μm in diameter were also made in the film. These microholes were used to measure parasitic radiation emitted by atoms colliding with the screen and not flying through subwavelength holes. These atoms emit radiation that can also propagate through nanoholes, producing a parasitic background against which a signal from atoms transmitted through holes is detected.

Measurements of photon transport by an atom through subwavelength holes were performed in the following way. A Rb atomic beam was directed on a screen with holes. Two laser beams focused by cylindrical lenses intersect the atomic beam directly in front of the screen and excite Rb atoms to the $5D_{5/2}$ state. The size of the region of interaction of atoms with laser radiation was 50 μm. The parameters of laser beams were chosen to provide single excitation of the atom to the $5D_{5/2}$ state during its flight. This was achieved at the Rabi frequencies $\Omega_{780} = 2\pi \times 100$ MHz and $\Omega_{776} = 2\pi \times 2$ MHz on the corresponding transitions.

Excited atoms transmitted through holes in the screen were detected on the other side of the screen by a fluorescence signal at 420 nm. The fluorescence signal was detected with a two-dimensional high-sensitivity EMCCD camera (Princeton Instruments). The screen with hole arrays was imaged by a high-numerical aperture lens ($NA = 0.54$) on the EMCCD array. The radiation collection solid angle was 0.48 sr. The two-dimensional EMCCD camera simultaneously detected fluorescence from atoms flying (1) through all subwavelength hole arrays in the screen, (2) through microholes 6 μm in diameter and also (3) the background signal through a part of the screen without holes.

By measuring the fluorescence signal from microholes, we determined the fluorescence of atoms in front of the screen and the photon transfer efficiency through a subwavelength hole. By detecting the fluorescence

signal through the screen without holes, we determined the contribution of the background fluorescence signal from excited Rb atoms in front of the screen.

The efficiency of photon transfer by an atom through a subwavelength hole was determined by measuring the fluorescence signal from atoms at 420 nm as a function of the distance $L$ between the screen and the excitation region. The results of these measurements are presented in Fig. 9. It can be seen from Fig. 9 that the fluorescence signal for all subwavelength holes increases with increasing $L$ and achieves its maximum for $L = 100$ μm. As the distance $L$ is further increased, the fluorescence signal from atoms transmitted through holes drastically decreases. This is explained by the fact that for a large distance between the atom and screen, the excited atom spontaneously decays to the ground state in front of the screen and therefore atoms transmitted through holes in the excited state are absent. As expected, such a decrease in the signal occurs at distances corresponding to the time of flight of the atom in the excited state, which is approximately 150 μm. The decrease in the fluorescence signal at distances smaller than 100 μm is explained by the decrease in the excitation region of atoms in front of the screen.

A signal obtained from arrays with subwavelength holes (Fig. 9) was compared with signals from the screen without holes and from microholes (6 μm in diameter). A comparison of signals from subwavelength holes with different diameters show that the florescence signal decreases more sharply with increasing distance for holes with the smaller diameter. This is explained by the fact that large holes also transmit parasitic radiation from atoms in front of the screen emitting at 420 nm. According to the Bethe theory, this background signal is stronger for holes with larger diameters. This leads to different decay rates of the fluorescence signal for different hole diameters in Fig. 9. The parasitic effect is most noticeable for holes with large diameter (540 nm) for which the signal has the "nonzero base" at large distances from the excitation region to the screen.

Figure 9 also presents the dependence of the fluorescence signal on the distance $L$ between the screen and excitation region for control microscopic holes (at the 1 : 100 scale). One can see that the dependence of the fluorescence signal on the distance for these holes is less sharp than for subwavelength holes. This is explained by the fact that in this case the signal contains fluorescence from all atoms: both excited atoms transmitted through the screen with holes and atoms that emitted photons in front of the screen. A comparison of signals from microholes and subwavelength holes convincingly proves the photon transfer by the atom through a subwavelength hole in the screen.

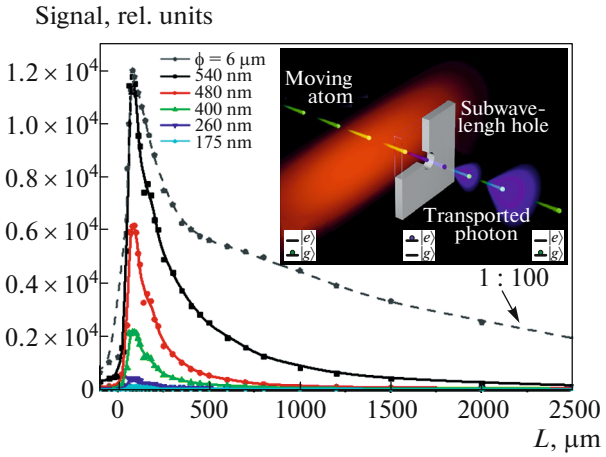


**Fig. 9.** (Color online) Fluorescence signal from atoms at 420 nm measured with a CCD as a function of the distance $L$ between the screen and excitation region. The dashed curve is a signal obtained from control holes 6 μm in diameter (the signal is 100 times reduced).

## 6. INTERACTION OF AN EXCITED ATOM WITH A SURFACE

Our measurements of the photon transport by an atom showed that the number of photons transferred in experiments was considerably smaller than the calculated number. Figure 10 shows the experimental dependence of the number $N_{\text{atom}}^{\text{photons}}$ of photons transferred by an atom on the diameter of a subwavelength hole and this dependence calculated by (4). For the hole diameter 175 nm, the signal becomes an unmeasurably small. The calculated dependence is described by the quadratic function of the hole diameter due to the linear dependence of the atomic flux on the hole area. The experimental dependence is different. The possible reason is considered below.

The efficiency of photon transfer by an atom flying through a hole is affected by its deexcitation inside the nanochannel. The flight of the excited atom through the hole in a metal screen is accompanied by the interaction of the atom with the screen material, which in turn can lead to the nonradiative deexcitation of the atom. The deexcitation probability of the atom near the material surface is determined by the properties of the atom and the physical and geometrical properties of the surface. The deexcitation of the atom near the metal surface includes the following processes [23]: (i) The interaction of the emitting atom with the surface plasmon–polariton modes of the metal screen; (ii) the interaction of the emitting atom with the waveguide modes of the subwavelength channel; (iii) self-interaction due to interaction of the emitting atom with the electromagnetic field reflected from the subwavelength channel surface; and (iv) nonradiative decay due to excitation of electron–hole pairs in the screen material.

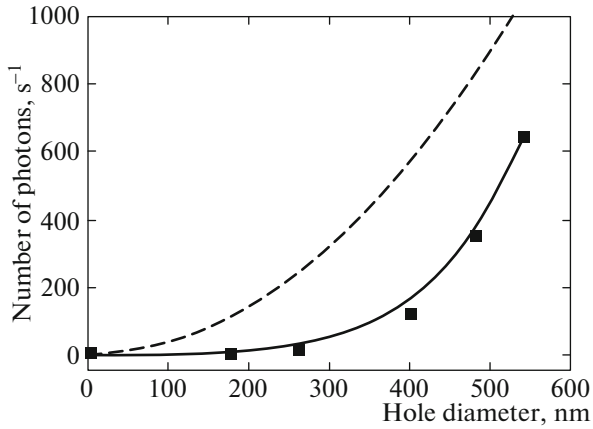


**Fig. 10.** Number of photons transferred by an atom measured as a function of the hole diameter; (squares) experiment, (dashed curve) theory.

The atom deexcitation effect can be taken into account by introducing the deexcitation coefficient $\chi(d)$ depending on the diameter $d$ of a subwavelength hole. Then, the number of transferred photons will be determined by the modified expression (4),

$$N_{\text{atom}}^{\text{photons}}(d) = \eta F S \chi(d). \tag{9}$$

The deexcitation coefficient $\chi(d)$ and its dependence on the subwavelength hole diameter can be determined by measuring the number of photons transferred by the atom through a control microscopic hole assuming that the fraction of atoms deexcited on channel walls during the flight through the microscopic hole ($d = 6$ μm) is negligibly small, i.e., $\chi(6\ \mu\text{m}) \equiv 1$.

The deexcitation coefficient $\chi(d)$ is determined by the expression

$$\chi(d) = \frac{N_{\text{ph}}^{\text{hole}} S^{6\mu\text{m}}}{N_{\text{ph}}^{6\mu\text{m}} S^{\text{hole}}}, \tag{10}$$

where $N_{\text{ph}}^{\text{hole}}$ and $N_{\text{ph}}^{6\mu\text{m}}$ are the numbers of photons per unit time transmitted through subwavelength holes and a control hole (6 μm), respectively; $S^{\text{hole}}$ and $S^{6\mu\text{m}}$ are the areas of corresponding holes. Note that this parameter is independent of the atomic flux, which is quite difficult to measure in experiments.

The analysis of previous studies of the deexcitation mechanism of quantum emitters near a surface shows that, despite numerous investigations performed in this research field, the deexcitation mechanism of a dipole near a surface remains unclear [24–29].

In the case of a dipole near a nanoparticle, deexcitation is related to dipole–dipole interaction of the dipole with its imaging on a metal surface. This theory explains experiments on fluorescence quenching for nanoparticles a few nanometers in size. However, the theory cannot explain fluorescence quenching for larger nanoparticles [30]. Theories based on the Gersten–Nitzan model [31–33] pretend to a more general description of experimental studies. However, their predictions are still far from complete coincidence with experimental data. Recently an attempt was made to improve the model by introducing empirical corrections to permittivities making them dependent on the nanoparticle size [30]. This improved the agreement with experimental data for particles with different diameters. However, these theories are based on the classical consideration of the interaction of a dipole with a material medium.

Based on [34], we estimate the deexcitation rate of an atom in our experiment. According to [34], the spontaneous decay rate $\Gamma$ of a dipole at a distance of $z$ from the silver surface can be written in the form

$$\Gamma = \frac{|d|^2}{12\pi\epsilon_0\hbar z^3} \sum_{i=A,B,C} F_i(z), \tag{11}$$

where

$$F_A = 8\frac{\omega_{\text{F}}}{\omega_p}\frac{1}{k_{\text{F}} l}\frac{\omega}{\omega_p},$$

$$F_B = 1.2\frac{\omega}{\omega_{\text{F}}}\frac{1}{k_{\text{F}} z},$$

$$F_C = 18\frac{\omega}{\omega_p}\frac{\omega_{\text{F}}}{\omega_p}\frac{1}{k_{\text{F}} z}.$$

Here, $|d|^2$ is the atomic transition dipole moment squared, $\omega_p$ is the plasma frequency of the material in the Drude model, $\omega_{\text{F}}$ is the Fermi frequency, $k_{\text{F}}$ is the Fermi wave vector, and $\epsilon_0$ is the electric constant. The last two terms in (11) determine the dependence of the spontaneous decay rate on the distance between the dipole and surface in the form $z^{-4}$, while the first term gives the dependence $z^{-3}$.

The fluorescence signal from atoms transmitted through subwavelength holes in the experiment is proportional to the number $N_{\text{ex}}$ of atoms transmitted through these holes remaining in the excited state. This quantity depends on the atom velocity $v$, the channel length $l$ and the hole diameter

$$N_{\text{ex}} \sim \int_0^R 2\pi z \exp\left(-\frac{\Gamma(z) l}{v}\right) dz. \tag{12}$$

Determining $N_{\text{ph}}^{\text{hole}}$ and $N_{\text{ph}}^{6\mu\text{m}}$ from (12) and using them in (10), we can find the deexcitation coefficient $\chi$. Figure 11 shows experimental and calculated dependences of the deexcitation coefficient $\chi$ on the hole diameter. Points show experimental data. The dashed curve corresponds to the calculated coefficient $\chi(d)$ defined by (11). Calculations involved the following relaxation channels of the atom from the excited state: $5D_{5/2} \to 6P_{3/2}$, $6P_{3/2} \to 5S_{1/2}$, $6P_{3/2} \to 4D_{5/2}$, $6P_{3/2} \to 4D_{3/2}$, and $6P_{3/2} \to 4S_{1/2}$. To compare experi-

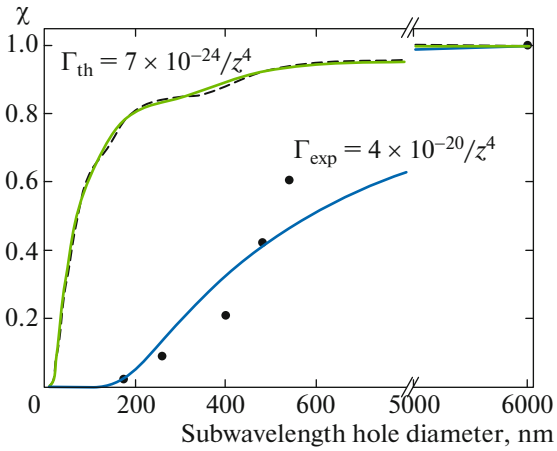


**Fig. 11.** (Color online) Experimental (black points) and calculated curves of the deexcitation coefficient $\chi$ on the diameter of subwavelength holes. The dashed curve is calculated for rubidium atoms. The green curve is calculated using approximation with a single decay parameter $\Gamma_{th} = 7 \times 10^{-24}/z^4$. Experimental values are approximated by the blue curve with the decay parameter $\Gamma_{exp} = 7 \times 10^{-20}/z^4$.

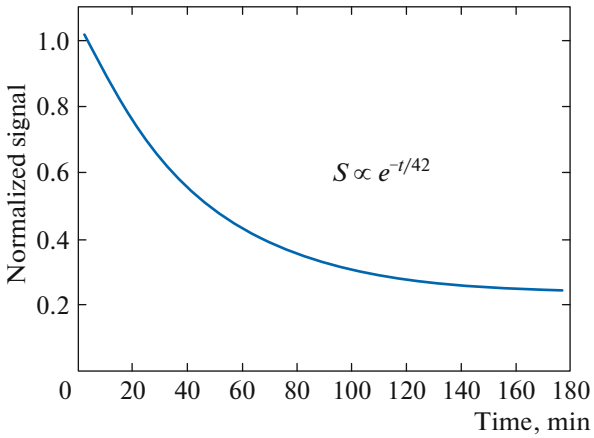


**Fig. 12.** (Color online) Experimental decrease in the fluorescence intensity of atoms caused by covering of a hole with Rb atoms during experiments.

mental results with calculations, we approximated our calculated curve by the dependence with one parameter, the decay rate. The best approximation was achieved for $\Gamma_{th} = 7 \times 10^{-24}/z^4$. One can see from Fig. 11 that the calculated and experimental dependences strongly differ. The decay rate obtained in experiments was $\Gamma_{exp} = 7 \times 10^{-20}/z^4$.

Such a strong difference between decay rates can be explained by two reasons. The first reason can be the model used for theoretical estimates [34]. This model takes into account only the stationary interaction of a dipole with a flat metal surface. This does not completely correspond to the experimental conditions of the flight of an atom through a subwavelength channel, where the atom can more strongly interact with the surface. In addition, the parameter $F_C$ was calculated assuming the zero temperature of the surface. Experimental conditions considerably differ from model conditions in the following: (i) interaction occurs not with a flat surface but with a cylindrical surface; (ii) interaction during the flight of an atom through a subwavelength hole is nonstationary; (iii) interaction occurs at room temperature.

The second reason may be a decrease in the holes diameter due to the deposition of Rb atoms on the holes. To verify this assumption, we studied the flight of atoms through subwavelength holes at long times (≈3 h) and found that the fluorescence signal from atoms transmitted through holes decreased with time (Fig. 12). The characteristic decay time caused by filling with rubidium atoms was 42 min.

Thus, theoretical and experimental data presented above suggest that for holes with diameters smaller than 200 nm, fluorescence quenching caused by the interaction of flying atoms with the screen material in a subwavelength channel should be observed. However, measurements preformed by the moment do not allow us to determine reliably the strength of this interaction, because holes are also partially covered by Rb atoms. In the future, we plan to modify our setup for eliminating the filling of holes with atoms, which will allow us to determine the deexcitation parameters of atoms interacting with the surface.

## 7. CONCLUSIONS

We have studied the localization and transfer of a single photon by a single atom through a subwavelength hole. This process was first proposed in [16]. The transfer mechanism is based on the reduction of the wave packet of a single photon due to its absorption by an atom resulting in its localization in a volume with linear dimensions much smaller than the radiation wavelength and the hole diameter. During the photon transfer, a single-photon, single-mode wave packet of laser light is transformed to a single-photon multimode wave packet in a free space. Each atom in this process transfers no more than one photon through a subwavelength hole. From this point of view, we are dealing with a nanolocalized source of single photons.

Our study has shown that the photon transfer efficiency depends on the hole size, the material of a screen in which the hole is made, the atom velocity and its energy level diagram. We have estimated the influence of the interaction of an excited atom flying through a subwavelength channel with the screen material. The estimate showed that for holes with diameters smaller than 200 nm, the quenching of the excited atom can affect the photon transfer efficiency.

The scheme of the photon transfer by an atom through a subwavelength channel opens up possibilities for studying new physical effects such as the inves-

tigation of Van der Waals forces in the interaction of a neutral atom with the screen material [35, 36] inside a cylindrical cavity [37] and the study of the interaction of excited atoms with plasmon nanostructures [38, 39]. In addition, the scheme can be used for studying quantum friction processes [40, 41].

In this paper, we have studied the flight of atoms by detecting photons at a wavelength of 420 nm. However, there exists another excitation decay channel $5D_{5/2} \rightarrow 5P_{3/2} \rightarrow 5S_{1/2}$ with emission of two photons at 776 and 780 nm. The two-photon decay channel in this scheme can be used for the development of a nanosize source for generating photon pairs [42].

## ACKNOWLEDGMENTS

The authors thank S.Yu. Alyatkin for his help at the initial stages of experimental studies and O.I. Tat'yanchenko for her help in preparation of the paper. The study was partially supported by the program "Nanoengineering of Plasmon Nanostructures and the Study of Their Optical Properties" of the Presidium of the Russian Academy of Sciences and by the Russian Foundation for Basic Research (grant no. 17-02-01093).

## REFERENCES

1. H. A. Bethe, Phys. Rev. **66**, 163 (1944).
2. A. Yu. Nikitin, D. Zueco, F. J. García-Vidal, and L. Martín-Moreno, Phys. Rev. B **78**, 165429 (2008).
3. R. Wannemacher, Opt. Commun. **195**, 107 (2001).
4. E. Popov, N. Bonod, M. Nevière, H. Rigneault, P.-F. Lenne, and P. Chaumet, Appl. Opt. **44**, 2332 (2005).
5. A. Degiron, H. J. Lezec, N. Yamamoto, and T. W. Ebbesen, Opt. Commun. **239**, 61 (2004).
6. P. N. Melentiev, A. E. Afanasiev, A. A. Kuzin, A. V. Zablotskiy, A. S. Baturin, and V. I. Balykin, Opt. Express **19**, 22743 (2011).
7. I. V. Treshin, V. V. Klimov, P. N. Melentiev, and V. I. Balykin, Phys. Rev. A **88**, 023832 (2013).
8. P. N. Melentiev, A. E. Afanasiev, A. A. Kuzin, A. V. Zablotskiy, A. S. Baturin, and V. I. Balykin, J. Exp. Theor. Phys. **115**, 185 (2012).
9. T. W. Ebbesen, H. J. Lezec, H. F. Ghaemi, T. Thio, and P. A. Wolff, Nature **391**, 667 (1998).
10. F. J. García-Vidal, L. Martin-Moreno, T. W. Ebbesen, and L. Kuipers, Rev. Mod. Phys. **82**, 729 (2010).
11. A. S. Vengurlekar, Curr. Sci. **98**, 1020 (2010).
12. F. J. García de Abajo, Rev. Mod. Phys. **79**, 1267 (2007).
13. L. Martín-Moreno, F. J. García-Vidal, H. J. Lezec, K. M. Pellerin, T. Thio, J. B. Pendry, and T. W. Ebbesen, Phys. Rev. Lett. **86**, 1114 (2001).
14. Z. Han and S. I. Bozhevolnyi, Rep. Progr. Phys. **76**, 016402 (2013).
15. T. V. Konstantinova, P. N. Melentiev, A. E. Afanasiev, A. A. Kuzin, P. A. Starikov, A. S. Baturin, A. V. Tausenev, A. V. Konyaschenko, and V. I. Balykin, Quantum Electron. **43**, 379 (2013).
16. A. E. Afanasiev, P. N. Melentiev, A. A. Kuzin, A. Yu. Kalatskiy, and V. I. Balykin, New J. Phys. **18**, 053015 (2016).
17. S. J. van Enk and H. J. Kimble, Phys. Rev. A **63**, 023809 (2001).
18. M. Stobińska, G. Alber, and G. Leuchs, Europhys. Lett. **86**, 14007 (2009).
19. T. T. Grove, V. Sanchez-Villicana, B. C. Duncan, S. Maleki, and P. L. Gould, Phys. Scripta **52**, 271 (1995).
20. S. Wielandy and A. L. Gaeta, Phys. Rev. A **58**, 2500 (1998).
21. O. S. Heavens, J. Opt. Soc. Am. **51**, 1058 (1961).
22. A. M. Akulshin, R. J. McLean, A. I. Sidorov, and P. Hannaford, Opt. Express **17**, 22861 (2009).
23. W. L. Barnes, J. Mod. Opt. **45**, 661 (1998).
24. B. N. J. Persson and N. D. Lang, Phys. Rev. B **26**, 5409 (1982).
25. R. J. Ruppin, Chem. Phys. **76**, 1681 (1982).
26. R. Carminati, J. J. Greffet, C. Henkel, and J. M. Vigoureux, Opt. Commun. **261**, 368 (2006).
27. S. Saini, G. Srinivas, and B. Bagchi, J. Phys. Chem. B **113**, 1817 (2009).
28. M. P. Singh and G. F. Strouse, J. Amer. Chem. Soc. **132**, 9383 (2010).
29. V. N. Pustovit and T. V. Shahbazyan, J. Chem. Phys. **136**, 204701 (2012).
30. C. J. Breshike, R. A. Riskowski, and G. F. Strouse, J. Phys. Chem. C **117**, 23942 (2013).
31. J. Gersten and A. Nitzan, J. Chem. Phys. **75**, 1139 (1981).
32. H. Mertens, A. Koenderink, and A. Polman, Phys. Rev. B **76**, 115123 (2007).
33. G. Colas des Francs, A. Bouhelier, E. Finot, J. C. Weeber, A. Dereux, C. Girard, and E. Dujardin, Opt. Express **16**, 17654 (2008).
34. B. N. J. Persson and S. Andersson, Phys. Rev. B **29**, 4382 (1984).
35. J. E. Lennard-Jones, Trans. Faraday Soc. **28**, 333 (1932).
36. D. Bloch and M. Ducloy, Adv. At. Mol. Opt. Phys. **50**, 91 (2005).
37. A. E. Afanasiev and V. G. Minogin, Phys. Rev. A **82**, 052903 (2010).
38. L. Stern, M. Grajower, and U. Levy, Nat. Commun. **5**, 4865 (2014).
39. S. A. Aljunid, E. A. Chan, G. Adamo, M. Ducloy, D. Wilkowski, and N. I. Zheludev, Nano Lett. **16**, 3137 (2016).
40. S. Scheel and S. Y. Buhmann, Phys. Rev. A **80**, 042902 (2009).
41. F. Intravaia, R. O. Behunin, and D. A. R. Dalvit, Phys. Rev. A **89**, 050101 (2014).
42. B. Srivathsan, G. K. Gulati, B. Chng, G. Maslennikov, D. Matsukevich, and C. Kurtsiefer, Phys. Rev. Lett. **111**, 123602 (2013).

*Translated by M. Sapozhnikov*